ISSN: 3029-0732

Research Article

Journal of Cardiovascular and Cardiology

Method of Evaluation of Straine to Estimate the Dysfunction of Heart Chambers of Patients with Asd

Sakovich VV[1*], Zabrodskaya TE[2] and Sadovsky MG[3]

[1]*Federal Center for Heart Surgery, Krasnoyarsk, Russia*

[2]*V.F. Voino-Yasenetsky Krasnoyarsk State Medical University, Krasnoyarsk, Russia*

[3]*Institute of computational modelling SB RAS, Krasnoyarsk, Russia*

[*]Corresponding author
Sakovich VV, Federal Center for Heart Surgery, Krasnoyarsk, Russia.

Received: May 08, 2026; **Accepted:** May 19, 2026; **Published:** May 25, 2026

ABSTRACT
During the dynamic observation of patients with congenital heart defects, an accurate dynamic assessment of heart failure manifestations is necessary. The study aimed to calculate the index of longitudinal myocardial deformation in patients with atrial septal defect in the presence of significant interference (acoustic noise), for example, when examining young children, when the examination is conducted during active behavior, crying, and restlessness. We used the indices of longitudinal myocardial deformation to establish the presence and severity of cardiac chamber dysfunction. The study was conducted in groups of pediatric patients with isolated secondary central atrial septal defect (ASD). The study was conducted on a Philips iE33 device. The obtained data were analyzed using a set of deep learning neural network architectures designed for image segmentation. The study was conducted on the U-net architecture. As a result of processing the video stream, it was possible to solve the problem of automatic segmentation of the heart walls with reference to key points in the image. The data obtained allows us to judge the presence and degree of dysfunction of the heart chambers.

Keywords: Cardiac Chamber Dysfunction, Strain Imaging, Atrial Dysfunction, Cardiac Mechanics

Introduction

Echocardiography is an ultrasound method of functional diagnostics used to determine the anatomical features and functional characteristics of the heart. Interpretation of echocardiographic images is a labor- and time-consuming process, and the examination method is operator- and device-dependent. A breakthrough in image analysis using artificial neural networks, which occurred in the 2010s, has automated image processing and reduced the time required to analyze the obtained data, as well as reduced intra- and inter-operator variability. Currently, the development and optimization of echocardiographic data processing methods using artificial neural networks is actively underway.

Atrial septal defect (ASD) is one of the most common congenital heart defects in the modern population, characterized by a communication between the right and left atria. The prevalence of ASD is 3.89 per 1,000 children and 0.88 per 1,000 adults. Surgical correction of this defect is performed across a wide age range (from 6 months to virtually any age). Indications for surgical treatment include the onset or worsening of the symptoms associated with this defect, such as heart failure and/or pulmonary arterial hypertension.

This study addresses the problem of automatically determining the longitudinal strain of the left and right atria. These values are planned to be used in the future as an indication for elective surgical correction of ASD. The specificity of this situation is that the study is often performed on children, including young children. A significant challenge in obtaining reliable echocardiographic data and subsequent interpretation in these cases is that the study is often conducted in conditions of active behavior, crying, and restlessness of the child, which causes the image to constantly shift along all three coordinate axes.

Literature Review

Atrial septal defect (ASD) is one of the most common congenital heart defects in the modern population. This anatomical anomaly can be accompanied by a variety of complications,

Citation: Sakovich VV, Zabrodskaya TE, Sadovsky MG. Method of Evaluation of Straine to Estimate the Dysfunction of Heart Chambers of Patients with Asd. J Cardiovas Cardiol. 2026. 4(2): 1-7. DOI: doi.org/10.61440/JCC.2026.v4.64

which explains the active interest in this problem among both practicing physicians and medical researchers. A review of publications from the past five years revealed a large number of studies devoted to this pathology.

Study examined the etiology and development of ASD, described the clinical presentation, possible treatment options, and patient management strategies, and explained strategies for a multidisciplinary team aimed at improving treatment outcomes, including through the development of appropriate patient communication strategies [1]. Article describes a comparative study of two surgical methods for treating ASD: median sternotomy and an anterolateral mini-thoracotomy approach [2]. In, children with atrial septal defects (ASDs) were examined to rule out associated vascular anomalies [3].

A group of authors assessed acute changes in ventricular longitudinal strain after transcatheter closure of atrial septal defects and evaluated their relationship with the size of the occlusion device [4].The magnitude of global right ventricular longitudinal strain was used as an important diagnostic indicator.

In, the use of the strain index was demonstrated to assess the impact of percutaneous atrial septal defect (ASD) closure on left ventricular (LV) function in adult patients [5].

Approaches to echocardiographic image processing using artificial neural networks were also analyzed. For example, in, the authors used a logic-transparent deep neural network to classify echocardiographic images, achieving an average classification accuracy of 98.2% [6]. A set of MENN convolutional neural networks is proposed for the analysis of left ventricular images in both long-axis (B-mode) and short-axis (M-mode) speckle tracking modes [7]. The effectiveness of the proposed architecture was further validated in two preclinical models, achieving excellent correlation between the results of automated and manual echocardiographic image analysis (Pearson's correlation coefficient r ranging from 0.85 to 0.99).

The use of a deep neural network with an attention mechanism and a residual feature aggregation module for left ventricular segmentation in transesophageal echocardiography images during cardiopulmonary resuscitation is described [8]. The goal of the study was to determine the optimal position for effective chest compression using left ventricular systolic function.

The possibility of detecting a history of myocardial infarction from echocardiographic recordings was demonstrated [9]. The model proposed by the authors is a pipeline consisting of two-dimensional convolutional neural networks that preprocess the data by segmenting the left ventricular cavity from the apical four-chamber approach. A three-dimensional convolutional neural network then performs binary heartbeat detection on the frame sequence. The model achieved high accuracy: 100% precision, 95% recall, and 97.2% F1 score.

Nizar M.H.A. and a group of authors solved the problem of tracking the aortic valve in an echocardiography frame sequence [10]. Two convolutional neural network architectures were used to solve the detection problem: a faster single-shot Multibox detector (solid-state drive) and a region-based convolutional neural network (RNN). Thus, it can be concluded that the topic chosen in the work is quite relevant in modern conditions and should be considered at the intersection of such sciences as medicine, cybernetics and computer science, from the point of view of the problems of artificial intelligence and computer vision.

Materials and Methods

Methods Used

To solve the stated problems, we used the Unet segmentation model, preprocessed images using Gaussian filtering methods, the Canny boundary operator, and standard OpenCV library procedures [11-14].

To calculate the longitudinal deformation of the myocardium, it is necessary to find the extreme (boundary) points of the analyzed atrium. This requires finding fragments of the atrial wall contour, which can be quite problematic due to strong noise in the region of interest. The upper and lower contours were found by identifying the maximum and minimum positions of the centroid of the closed contour, followed by finding the leftmost point of the upper contour fragment and the lowest point of the lower contour fragment.

After obtaining the values of the distance vector length between the extreme points, an averaging filter was used to smooth out deviations caused by errors in the labeling of the cardiac muscle contours. The strain parameters were calculated using formula (1):

$\varepsilon(t)=(L(t)-L(t_0))/(L(t_0))$, (1)

where L(t) is the distance between the extreme points of the current frame (end-systolic size of the myocardial segment), L(t0) is the length of the distance vector between the extreme points of the previous frame (end-diastolic size of the myocardial segment).

Experimental Materials

To develop an algorithm for calculating the atrial deformation parameter, a two-dimensional echocardiography video fragment must be preprocessed. Transthoracic echocardiography video recordings of 40 patients diagnosed with atrial septal defect (ASD) were used to segment the atrial walls and calculate deformation indices. The patients ranged in age from 0 to 18 years.

Based on these data, indications for surgical correction of the defect were determined. The study was conducted at the Federal Center for Cardiovascular Surgery in Krasnoyarsk.

The original resolution of the video fragments was 1344x1000 pixels, 25 frames per second, and RGB color encoding. The ECHO recordings, performed on a Philips iE33 system, contained significant noise. After removing unnecessary fragments, the image resolution became 800x600 pixels in RGB color encoding. Example images are shown in Figure 1.

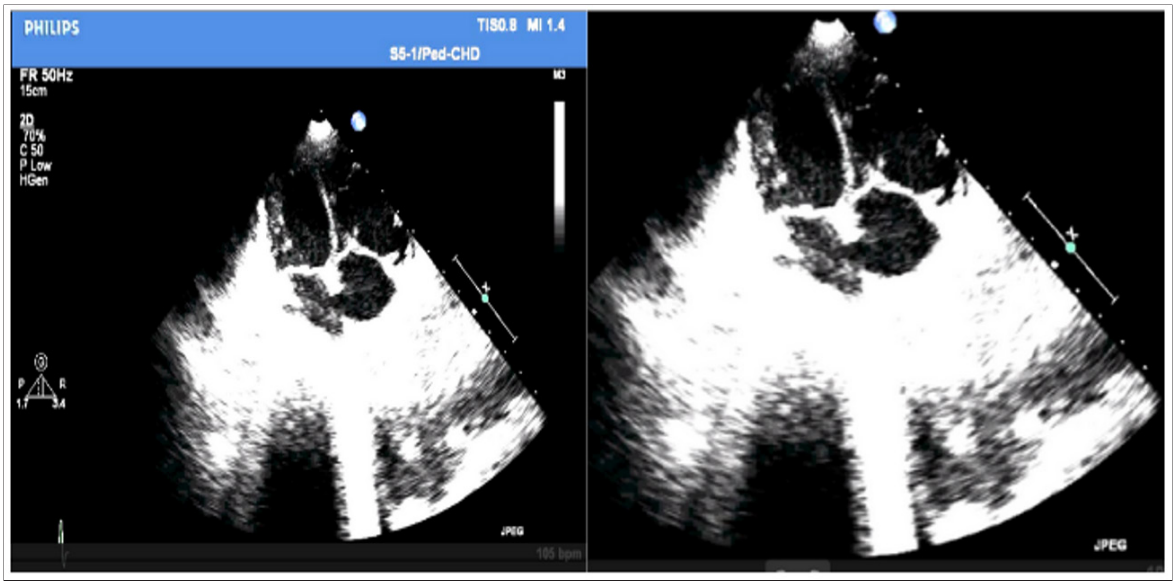

Figure 1: The original video fragment resolution is 1344x1000 pixels. An example of frame fragmentation for preparing neural network training

The fragmented images were annotated by expert physicians specializing in functional diagnostics, who manually labeled the area of the right and left atria by the "atria" class as a region of interest for further training of the neural networks. For model training, the sample was divided into training, validation, and test samples in a 70%:20%:10% ratio. As a result, the following sample was obtained: 1,500 images of patients' hearts in motion (1 contraction cycle) in the data set. 3,000 were labeled as atria (left and right). Figure 2 shows an example of manual labeling of atrial elements and obtaining a common "mask" (schematic contour) for further training of the neural network. The data set was labeled using the Labelme labeling program [15].

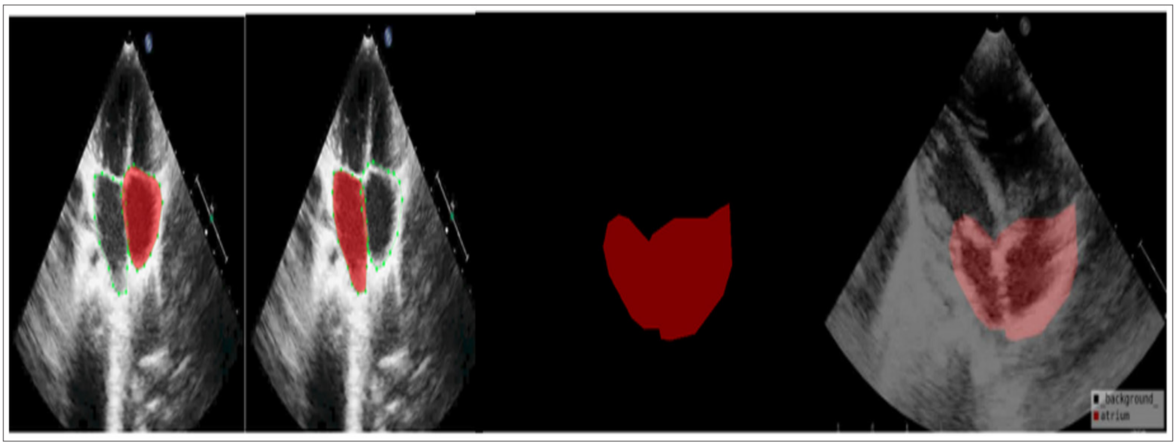

Figure 2: Marking of the atria on the image, where 1) the "mask" of the right atrium, 2) the "mask" of the left atrium, 3) the general "mask" of both atria, 4) addition of the image of the heart and the general "mask" of the atria.

Results

Segmentation Model Training Results

The model, based on the Unet convolutional neural network architecture, has a total of 6,502,786 neurons, 4,658,882 of which are trainable [11]. The neural network input contains 512x512 RGB pixels. After segmentation by the model, the image size is increased to the size of the analyzed video fragment, in this case, to 800x600 RGB pixels. The full structure of the created model is shown in the figure. Training was conducted in 18 epochs, with 147 iterations per epoch and a tensor dimension of 32 images. The training loss was 0.013 (val_loss0.017). The loss function was SparseCategoricalCrossentropy.

Layer (type)	Output Shape	Param #	Connected to
input_13 (InputLayer)	[(None, 512, 512, 3)]	0	[ ]
model_8 (Functional)	[(None, 256, 256, 96), (None, 128, 128, 144), (None, 64, 64, 192), (None, 32, 32, 576), (None, 16, 16, 320)]	1841984	[‘input_13[0][0]’]
sequential_25 (Sequential)	(None, 32, 32, 512)	1476608	[‘model_8[0][4]’]
concatenate_11 (Concatenate)	(None, 32, 32, 1088)	0	[‘sequential_25[0][0]’, ‘model_8[0][3]’]
sequential_26 (Sequential)	(None, 64, 64, 256)	2507776	[‘concatenate_11[0][0]’]
concatenate_12 (Concatenate)	(None, 64, 64, 448)	0	[‘sequential_26[0][0]’, ‘model_8[0][2]’]
sequential_27 (Sequential)	(None, 128, 128, 128)	516608	[‘concatenate_12[0][0]’]
concatenate_13 (Concatenate)	(None, 128, 128, 272)	0	[‘sequential_27[0][0]’, ‘model_8[0][1]’]
sequential_28 (Sequential)	(None, 256, 256, 64)	156928	[‘concatenate_13[0][0]’]
concatenate_14 (Concatenate)	(None, 256, 256, 160)	0	[‘sequential_28[0][0]’, ‘model_8[0][0]’]
conv2d_transpose_31 (Conv2DTranspose)	(None, 512, 512, 1)	1441	[‘concatenate_14[0][0]’]

Figure 3: Architecture of the trained model based on the Unet architecture.

Image Preparing for Strain Calculation

Video fragments from the Philips iE33 device with a duty cycle (image generation frequency) of 5-10 are fed into the automatic strain calculation system. The video image size is 1344x1000 pixels in the RGB color channel. A fragment with a 600x800 pixel window in the RGB color channel is extracted from the video stream. The resulting image is downsized to the input layer of the trained U-net neural network (512x512 pixels), resulting in segmented contours (“masks”) of the right and left atria. The image and “mask” are then convolved, resulting in an image of the segmented regions measuring 800x600 pixels in RGB color encoding. To further search for contours, the following operations were performed: conversion to grayscale, Gaussian filtering with an 11x11 pixel window to remove coarse noise, and contour search using the Canny operator with a parameter of 30, 150. Since the image is very noisy, most of the contours are unclosed. To solve this problem, the pixel value was supplemented with a dilation function [16]. The result of the operation is closed fragments of the visible atrial wall, prepared for deformation calculation. Figure 4 shows a step-by-step description of the image preprocessing procedure.

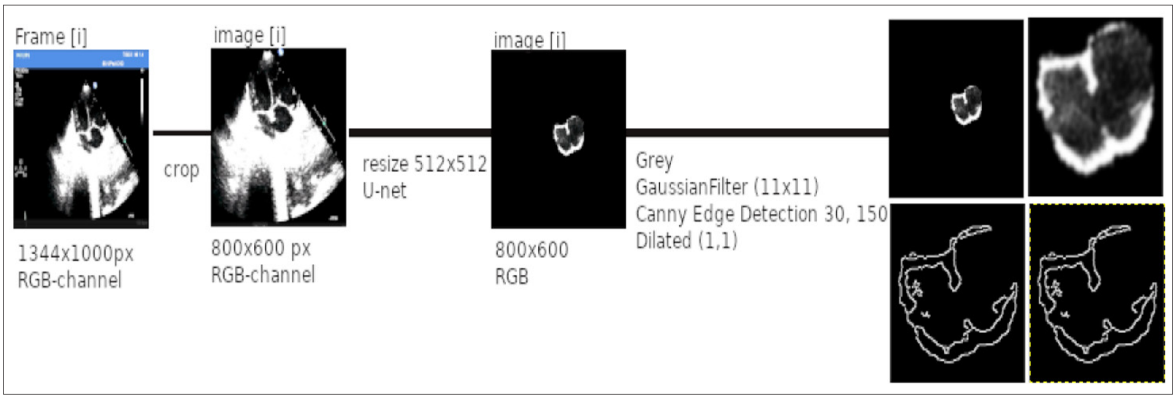

Figure 4: Algorithm for selecting the contour of the region of interest of the heart.

Calculating the Left Atrium Strain

After obtaining the atrial contour, it is necessary to find and record the extreme upper and lower points of the analyzed region. Because ultrasound images contain varying degrees of noise, precise location of the cardiac compartment boundaries is not always possible. Figure 5 shows examples of contours obtained with varying degrees of noise in the region of interest.

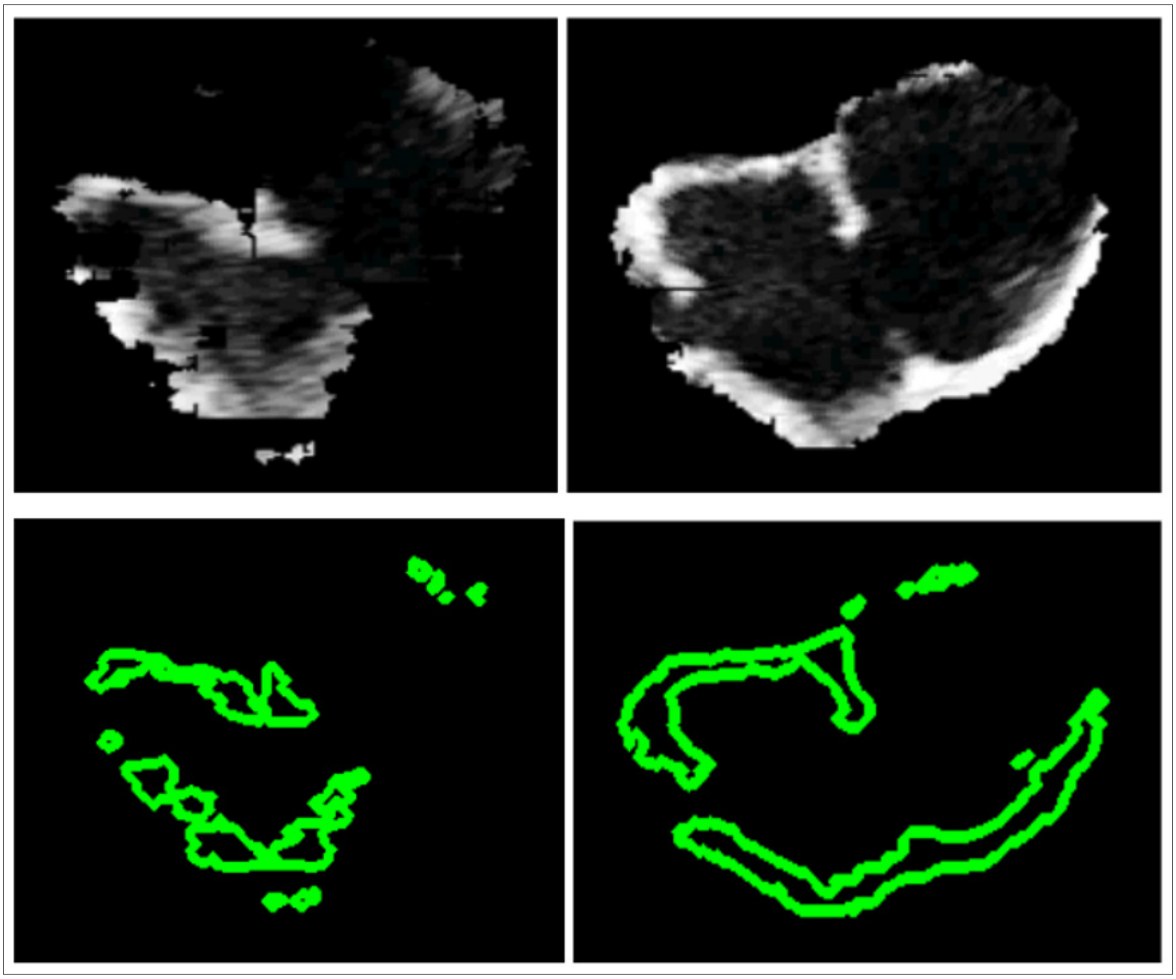

Figure 5: After obtaining the atrial contour, it is necessary to find and record the obtained result. Examples of contour extraction from echocardiography video frames: on the left is a "highly noisy" region of the atria, on the right is a noise-free region of the atria.

After finding the extreme points of the required contour fragments, the length of the resulting distance vector is calculated. Fig. 6 shows the point search results and the resulting vector. The red dot is the left extreme point of the superior fragment of the left atrial wall, the green dot is the inferior point of the inferior fragment of the left atrial wall, the green frame is the bounding box of the resulting closed contour, and the pink line is the distance vector between the extreme points.

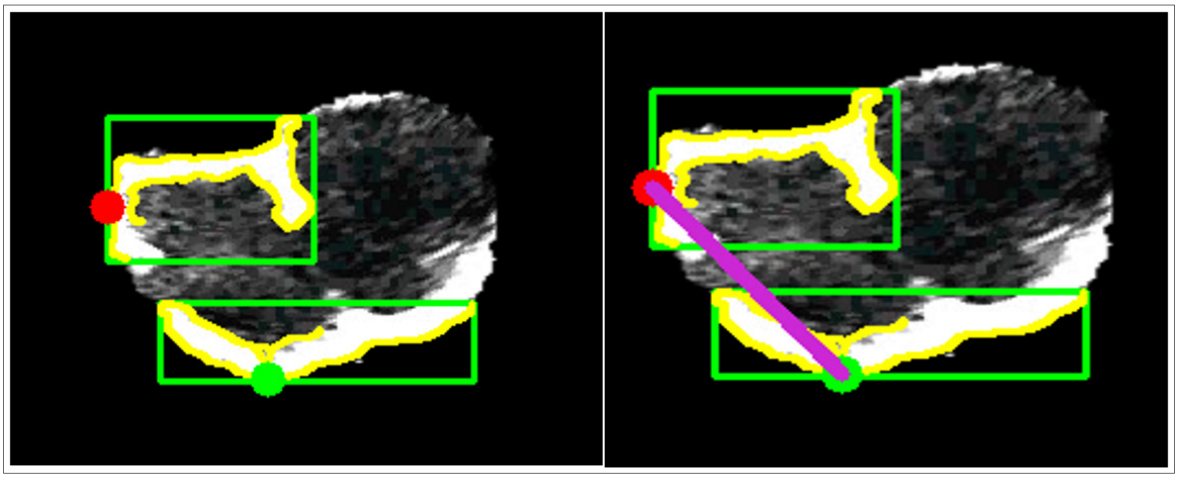

Figure 6: Result of searching for extreme points of visible sections of the walls of the left atrium.

Calculating Instantaneous and Average Left Atrium Strain

After generating a [[frame_number],[length]] list, the data was sorted in ascending order and copied into a one-dimensional ordered array. A median filter was then used to remove acoustic noise in the data obtained after calculating the length of the distance vector between the extreme points. After obtaining a noise-free signal, the instantaneous strain value was calculated using formula 1. For better understanding, the obtained data were converted to percentages. Table [1] presents the strain calculation results for one left atrial contraction cycle, the obtained data arrays, and the stages of their transformation.

Table 1: Step-By-Step Protocol for Calculating Instantaneous Strain Values

Frame number	Original length	After filtering with a median filter	Instantaneous strain value	Instantaneous strain value, %
0	75.610	75.610	0	+0
1	100.004	75.610	0.322	+32
2	52.325	100.004	-0.395	-40
3	121.490	60.440	0.514	+51
4	60.440	91.547	-0.339	-34
5	91.547	60.440	0.032	+3
6	58.051	62.393	0	+0
7	62.393	62.393	0.613	+61
8	112.445	100.687	0	+0
9	100.687	100.687	0	+0
10	80.529	100.687	0.010	+1
11	108.756	101.710	0	+0
12	101.710	101.710	0.010	+1
13	38.948	85.023	0	+0
14	85.023	55.901	-0.164	-16
15	55.901	85.023	-0.342	-34
16	102.004	102.004	0.520	+52
17	128.082	102.004	0.199	+20
18	58.034	123.709	0	+0
19	123.709	111.072	0.212	+21
20	111.072	123.709	-0.102	-10
21	150.416	111.072	0.113	+11
22	49.040	91.005	-0.102	-10
23	91.005	91.005	-0.180	-18
24	130.667	91.005	0	+0
25	10	100.498	0	+0
26	100.498	93.005	0.104	+10
27	93.005	93.005	-0.074	-7
28	67.601	93.005	0	+0

Figure 7 shows the graphs of the obtained data and the stages of their transformation.

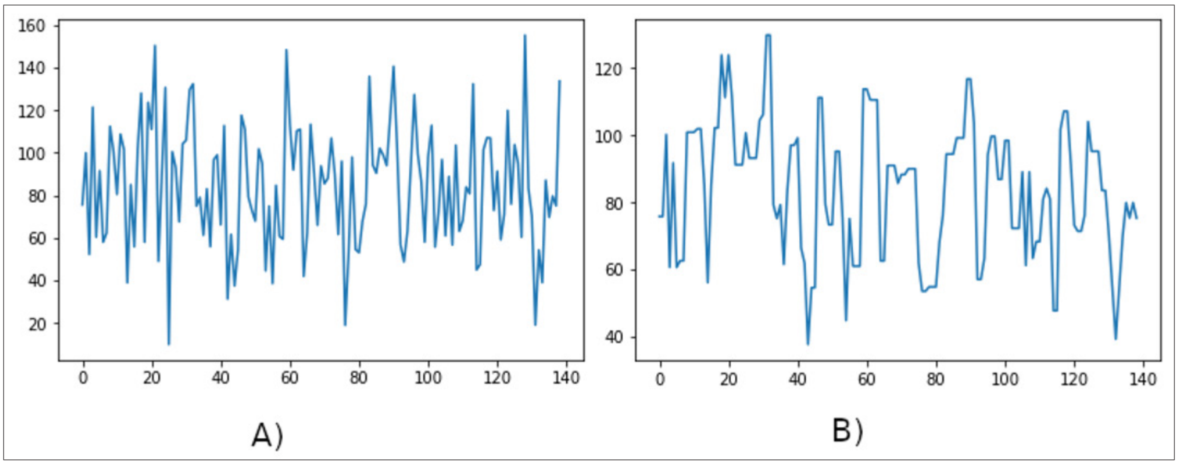

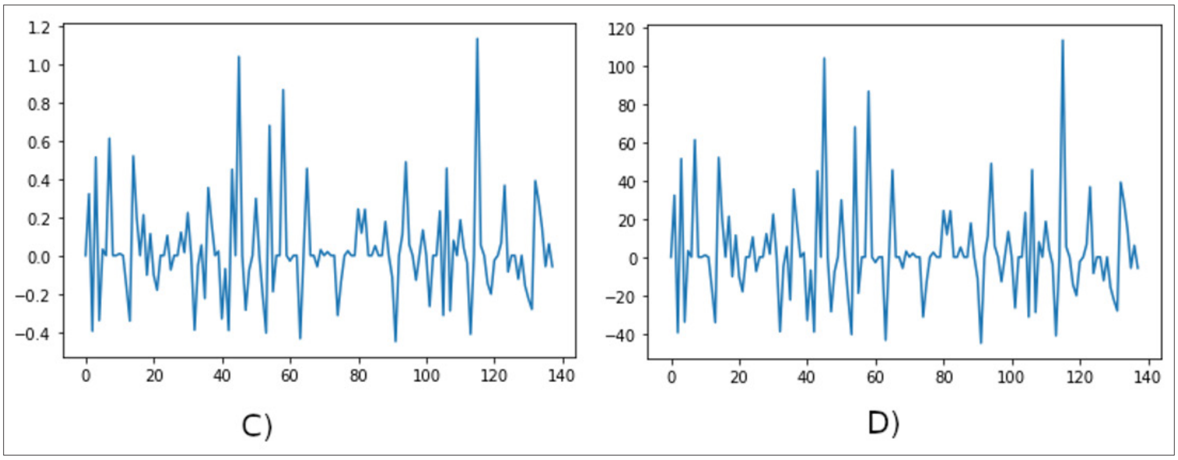

Figure 7: Graphs of deformation calculation, where A) is the graph of the initial data, B) is the graph of the data using the median filter, C) is the graph of the instantaneous deformation, D) is the percentage display of the instantaneous deformation.

Conclusion

The authors believe that the new parameter (atrial longitudinal strain) will enable functional diagnosticians and cardiologists to more accurately and precisely determine the optimal timing for planned ASD correction. We believe it would be appropriate to include myocardial longitudinal strain parameters in echocardiography protocols, particularly during the follow-up of children with ASD.

A promising approach from the perspective of applied information technology is to address the problem of strong acoustic noise (interference) when determining the contours of the left and right atria in echocardiography images. To address this issue, the authors plan to use a method for reconstructing the atrial wall using generative adversarial networks (GANNs). This will allow for the calculation of independent instantaneous and average strain parameters for both atria, thereby more accurately diagnosing cardiac chamber dysfunction, such as ASD.

References

1. Elsaka O. Pathophysiology, Investigations, and Management of Atrial Septal Defect Asian J. Med. Princ. Clin. Pract. 2021. 4: 207-220.
2. Bhattarai A, Paudel BS, Shah S, Pandey A, Khakural P, et al. Atrial Septal Defect Closure Via Mini Thoracotomy and with Peripheral Cannulation. J. Nepal Health Res. Counc. Nepal, 2021. 19:725-729.
3. Akbar A, Hussain I, Wazir HD, Rehman Y, Ilyas S, et al. Pattern of Vascular Anomalies Associated With Sinus Venosus Atrial Septal Defect Cureus. 2022. 14.
4. Alkhateeb A, Roushdy A, Hasan-Ali H, Kishk YT, El Sayegh A, et al. Impact of atrial septal defect device size on biventricular global and regional function: a two-dimensional strain echocardiographic study Cardiol. Young. 2022. 32: 746-754.
5. Miki T, Yamano T, Yamano M, Nakamura T, Takamatsu K, et al. Favorable changes of left ventricular function in the circumferential direction following transcatheter atrial septal defect closure: a strain imaging study Int. J. Cardiovasc. Imaging. 2021. 37: 903-912.
6. Huang M, Lin WC, Chen YD, Hsiao TA, Liu PY, et al. Explainable deep neural network for echocardiography view classification Eur. Hear. Journal - Cardiovasc. Imaging. 2022. 23.
7. Duan C, Montgomery MK, Chen X, Ullas S, Stansfield J, et al. Fully automated mouse echocardiography analysis using deep convolutional neural networks Am. J. Physiol. Circ. Physiol. 2022. 323: H628-H639.
8. Kang S, Kim SJ, Ahn HG, Cha KC, Yang S. Left ventricle segmentation in transesophageal echocardiography images using a deep neural network PLoS One / ed. Liu X. 2023. 18: e0280485.
9. Hamila O, Ramanna S, Henry CJ, Kiranyaz S, Hamila R, et al. Fully automated 2D and 3D convolutional neural networks pipeline for video segmentation and myocardial infarction detection in echocardiography Multimed. Tools Appl. 2022. 81: 37417-37439.
10. Nizar MH, Chan CK, Khalil A, Yusof AK, Lai KW. Real-time Detection of Aortic Valve in Echocardiography using Convolutional Neural Networks Curr. Med. Imaging Former. Curr. Med. Imaging Rev. 2020. 16: 584-591.
11. Ronneberger O, Fischer P, Brox T. U-Net: Convolutional Networks for Biomedical Image Segmentation. 2015.
12. Andrews J. Low-Pass Risetime Filters for Time Domain Applications. 2023.
13. Canny J. A Computational Approach to Edge Detection IEEE Trans. Pattern Anal. Mach. Intell. 1986. 8: 679-698.
14. OpenCV [Electronic resource]. URL: https://opencv.org/.
15. LabelMe [Electronic resource]. URL: http://labelme.csail.mit.edu/Release3.0/.
16. Eroding and Dilating [Electronic resource] // Open Source Computer Vision. URL: https://docs.opencv.org/3.4/db/df6/tutorial_erosion_dilatation.html.